Supplemental Material for

Paradoxical signaling regulates structural plasticity in dendritic spines

Padmini Rangamani[1*], Michael G. Levy[2], Shahid Khan[3], and George Oster[4]

[1] Department of Mechanical and Aerospace Engineering,
University of California San Diego, La Jolla CA 92093

[2] Biophysics Graduate Program, University of California Berkeley,
Berkeley CA 94720

[3] Molecular Biology Consortium, Lawrence Berkeley National Laboratory,
Berkeley CA 94720

[4] Department of Molecular and Cell Biology, University of California Berkeley,
Berkeley CA 94720.

[*] To whom correspondence should be addressed: padmini.rangamani@eng.ucsd.edu.

A brief introduction to modeling chemical reactions

Mass-action kinetics

We generate an ordinary differential equation (ODE) for each species using mass-action kinetics for each reaction. Under mass action, the rate of a chemical reaction is proportional to the product of the reactant concentrations raised to the power of their stoichiometric coefficients. For example, consider the one-reaction system:

$$X + Y \rightleftharpoons 2Z, \tag{S1}$$

where the forward and backward rates are k_1 and k_2. The differential equations describing the dynamics of species X, Y, and Z under mass-action kinetics are:

$$\begin{aligned} \frac{d[X]}{dt} &= k_2[Z]^2 - k_1[X][Y] \\ \frac{d[Y]}{dt} &= k_2[Z]^2 - k_1[X][Y] \\ \frac{d[Z]}{dt} &= k_1[X][Y] - k_2[Z]^2. \end{aligned} \tag{S2}$$

Michaelis-Menten kinetics

When the reaction is catalyzed by an enzyme, with kinetic properties k_{cat} and K_M,

$$\mathrm{S} \xrightarrow{\mathrm{E}} \mathrm{P},$$

then the reaction rate is given by

$$\frac{d[S]}{dt} = -\frac{k_{cat}[E][S]}{K_M + [S]} = \frac{d[P]}{dt} \tag{S3}$$

Paradoxical signaling

One-Tier Model of Paradoxical Signaling

The phenomenological model underlying the activation-inhibition loop shown in Figure S2A can be written as a system of ordinary differential equations (ODEs) to track the temporal dynamics of the response function R due to time-dependent stimulus input $S(t)$ (details in Table S1). The activator A and inhibitor I, transmit information from the stimulus to the response. * indicates the activated fraction of the species. Using mass-action kinetics, we can formulate a system of ODEs to represent the change in concentration of each species over time. Since $A(t)$ and $I(t)$ are immediate effectors of the stimulus $S(t)$, they demonstrate a rapid increase in activation and decay exponentially (Figure S2A, B). The response $R(t)$ shows a slightly delayed peak compared to $A(t)$ and $I(t)$, which is consistent with degree of separation of $R(t)$ from $S(t)$. The dynamics of each of these components follows a biexponential function, which is sufficient to explain the

time scales of activation and inhibition. These results suggest that changing the parameters of the above model is sufficient to reproduce all the results of the temporal dynamics of spine volume change coupled with CaMKII and RhoGTPases [19].

Under the assumption of mass action kinetics, the rate of a chemical reaction is proportional to the product of the reactant concentrations raised to the power of their stoichiometric coefficients. For the simple paradoxical signaling network shown in Figure S2A, the dynamics can be modeled using the reactions in Table S1. k_i's represent the forward reaction rates. For simplicity, we ignore the backward reaction rate here; including the reverse reaction will not affect the qualitative behavior of the system. S is a controlled, time-dependent input, a pulse function, to model the burst of calcium into the spine. The system of ordinary differential equations resulting from this system are given in Eq. S4 and were solved using the ode45 routine in MATLAB (Mathworks, Natick, MA) (Figure S1B). It is straightforward to note that this simple system gives rise to the behaviors observed in the spine dynamics but also in many other signaling systems [1, 8, 7].

Table S1: Reactions for a one-tier activation-inhibition loop

Initial concentrations (all in μM): [A] =A_0; [I] = I_0; [R] = R_0

Reaction	k_{on}	Notes
A + S $\rightarrow$ A*	k_1	Stimulus activates activator
A* + R $\rightarrow$ R*	k_2	Response is activated by A
I + S $\rightarrow$ I*	k_3	Stimulus activates inhibitor
R* + I* $\rightarrow$ R	k_4	Response in inhibited by I

The corresponding differential equations are given as

$$\begin{aligned}
\frac{d[A]}{dt} &= -k_1[A]S(t) \\
\frac{d[A^*]}{dt} &= k_1[A]S(t) - k_2[A^*][R] \\
\frac{d[I]}{dt} &= -k_3[I]S(t) \\
\frac{d[I^*]}{dt} &= k_3[I]S(t) - k_4[I^*][R^*] \\
\frac{d[R]}{dt} &= -k_2[A^*][R] + k_4[I^*][R^*] \\
\frac{d[R^*]}{dt} &= k_2[A^*][R] - k_4[I^*][R^*]
\end{aligned} \tag{S4}$$

Multi-tier model of paradoxical signaling

Table S2: Reactions for a multi-tier activation-inhibition loop

Initial concentrations (all in μM): [A] $=A_0$; [I] $= I_0$; [R] $= R_0$		
Reaction	k_{on}	Notes
$A_1 + S \rightarrow A_1^*$	k_1	Stimulus activates activator 1
$A_1^* + A_2 \rightarrow A_2^*$	k_2	Activator 1 activates activator 2
$A_2^* + R \rightarrow R^*$	k_3	Response is activated by activator 2
$I_1 + S \rightarrow I_1^*$	k_4	Stimulus activates inhibitor 1
$I_2 + I_1^* \rightarrow I_2^*$	k_5	Inhibitor 1 activates inhibitor 2
$R^* + I_2^* \rightarrow R$	k_6	Response is inhibited by inhibitor 2

The reactions for the multi-tier paradoxical signaling are given in Table S2, where k_i's represent the forward reaction rates. S is a controlled, time-dependent input, a pulse function, to model the burst of calcium into the spine. The system of ordinary differential equations resulting from this system are given in Eq. S5 and were solved using the ode45 routine in MATLAB (Mathworks, Natick, MA).

$$\begin{aligned}
\frac{d[A_1]}{dt} &= -k_1[A_1]S(t) \\
\frac{d[A_1^*]}{dt} &= k_1[A_1]S(t) - k_2[A_1^*][A_2] \\
\frac{d[A_2^*]}{dt} &= k_2[A_1^*][A_2] - k_3[A_2^*][R] \\
\frac{d[I_1]}{dt} &= -k_4[I_1]S(t) \\
\frac{d[I_1^*]}{dt} &= k_4[I_1]S(t) - k_5[I_1^*][I2] \\
\frac{d[I_2^*]}{dt} &= k_5[I_1^*][I_2] - k_6[I_2^*][R^*] \\
\frac{d[R]}{dt} &= -k_3[A_2^*][R] + k_6[I_2^*][R^*] \\
\frac{d[R^*]}{dt} &= k_3[A^*][R] - k_6[I^*][R^*]
\end{aligned} \tag{S5}$$

We summarize our observations from the toy models here: in the case of a simple biexponential function Eq.3, it is straightforward to see how the two exponents, a and b, characterize the inhibition and activation dynamics respectively. In the case of dynamics regulated by large signaling networks, a and b are no longer

constants but regulated by upstream processes and activity of proteins. Nonetheless, this simple function gives us large insight into how homeostasis might come about. Further extending this idea to that of a one-tier paradoxical signaling model and subsequently the two tier model gives us a way of understanding how the kinetic parameters influence the time courses (Figure S1B). Effectively, the large network shown in Figure 2C is a larger scale system with the same dynamic behavior.

Model development for spine volume change

CaMKII Module

The reactions in the CaMKII module are based on the events outlined in the Introduction section of the main text. NMDA receptor activation leads to a Ca^{2+}pulse, which then binds to Calmodulin, resulting in a calcium-calmodulin complex. This complex is key for the activation of CaMKII by binding to the kinase and relieving the autoinhibition. The structural details of how this happens are discussed in [28, 6] and are beyond the scope of the current work. An additional key step in the activation of CaMKII is autophosphorylation. To represent these kinetics, we have used the model developed by Pi and Lisman [23]. Calcium-calmodulin also activates calcineurin, also known as PP3. Calcineurin acts through a cascade of phosphatases I1 and PP1 to dephosphorylate CaMKII [18]. The calmodulin levels are regulated by a protein called neurogranin, which is found in large quantities in the brain [36]. The kinetics of PP1 activity are described in [23]. Continuous activation of CaMKII does not occur for the majority of the CaMKII population since the calcium pulse is transient and the activated CaMKII is dephosphorylated. Only CaMKII bound to the NMDA receptors in the PSD is persistently activated.

Cdc42 Module

Cdc42 is a small RhoGTPase, which plays an important role in governing the actin remodeling events. It is required for the activation of WASP through PIP2 and the subsequent downstream activation of Arp2/3 [27]. The activity of Cdc42 is regulated by Guanine nucleotide exchange factors (GEFs) and GTPase activating proteins (GAPs). There are a large number of GEFs and GAPs present in the brain and their activity is known to be controlled directly or indirectly though CaMKII. We assumed that the GEFs and GAPs were activated by CaMKII (based on [22]) and were inactivated by PP1. Since phosphatases are known to be promiscuous [34], this assumption is justified. The GTP bound Cdc42 then activates WASP and Arp2/3 [26, 15, 10].

Cofilin Module

Cofilin is an important regulator of actin dynamics; by severing actin filaments, it plays an important role in recycling the actin [30]. Cofilin is known to be negatively regulated by phosphorylation mediated by LIM kinase [4] and activated by dephosphorylation by SSH1 [4]. We use the module developed in [26] to model cofilin dynamics. SSH1 itself is activated by calcineurin [35] and inhibited by CaMKII. LIM kinase is activated by Rho kinase, ROCK [2]. The cofilin that is activated by these events leads to the severing of actin filaments and is modeled using f_{sev} (Table S6) based on the model presented in [31].

Actin module and pushing velocity

We use the well-mixed model developed by Tania *et. al.* [31] with a few modifications, to model the dynamics of the barbed end generation from Arp2/3 and cofilin activity. The phosphorylation of CaMKII releases F-actin and G-actin in the spine, which are then free to generate barbed ends through filament nucleation and severing. The degradation and aging of filaments results in regeneration of G-actin. However, it has been shown that the main mode of actin remodeling is through the creation of short branches and therefore through nucleation and that the mature spine does not have long filaments [32, 11]. Therefore, we only included actin branch nucleation and barbed end generation (pushing and non-pushing) in our model. It has also been separately shown that G-actin is buffered by the G-actin pool in the dendritic shaft and this serves as an infinite source and the fast diffusion of G-actin between the spine and the shaft buffers the spine G-actin concentration [13].

The functional forms of severing and nucleation are taken from [31]. The barbed ends are capped at a fixed rate k_{cap}. Not all barbed ends generate a pushing velocity; the relationship between the pushing barbed ends Bp, and the total barbed ends is derived from the conservation conditions in [31]. As explained in [31], Eq. S6 ensures that spine expansion is initiated only when barbed ends have built up sufficiently. The actin-mediated spine growth events are modeled as an elastic Brownian ratchet [16, 17]. The difference between our model and the one published in [31] is that the species involved in the actin module are all regulated by upstream signaling regulated by CaMKII.

The relationship between pushing barbed ends, Bp, and the membrane velocity has been derived in [14, 31], and is used here to calculate the radius of the growing spine in response to the actin remodeling events. This relationship is given as

$$V_{mb} = V_0 \frac{Bp}{Bp + \phi \exp(\omega/Bp)} \tag{S6}$$

Here, we used the values of $\phi = 10/\mu m$, and $\omega = 50$ per μm. [31]. ϕ is the geometric parameter used in computing membrane protrusion rate and ω is the physical parameter describing the membrane resistance [31, 14]. This density-velocity relationship has a biphasic behavior – for a small number of barbed ends, the membrane resistance limits the velocity, explained as 'decoherent' regime in [14] and for large barbed end density, or the 'coherent' regime, the protrusion rate is not sensitive to the number of barbed ends.

Rho-Myosin Module

Rho is known to regulate ROCK and therefore myosin activity. In cell motility models, Rho is known to play an important role in contractility. Here, we apply the idea of myosin-mediated contraction that is governed by RhoGTP activity. Rho is a small GTPase and as in the Cdc42 module, we assume that the GEF and GAP activity are regulated by the CaMKII module. RhoGTP then activates ROCK, which is known to activate both myosin light chain kinase and myosin light chain phosphatase [12]. The reactions and reaction rates for ROCK activation of myosin light chain are based on the model presented in [12].

Spine radius

We propose the following equation for the dynamics of the spine volume.

$$\frac{dR}{dt} = V_{mb} - k_{shrink}[MLC^*]R \tag{S7}$$

The spine growth velocity is assumed to depend on the pushing velocity generated by actin and the shrinkage of the spine is proportional to the amount of myosin light chain that is phosphorylated and the radius of the spine. A similar model force dependence on myosin concentration for contractility was proposed in [3].

Actin depolymerization or myosin-mediated contraction?

Actin depolymerization is another key factor in actin remodeling. An open question in the field is whether increasing actin depolymerization is sufficient to induce spine contraction. In order to study the effect of actin depolymerization, we included another term in the conversion of F-actin to G-actin, which had the rate $k_{depol}[F-actin]$. The number of pushing barbed ends is affected by depolymerization (Figure S8A), however for rates of depolymerization as observed in experiments [25] and used in other models [17], the spine dynamics is not greatly affected (Figure S8B). More importantly, our conclusion that if the barbed ends are sufficient to drive the velocity to a coherent regime, then the spine dynamics is robust, still holds. Also, if the depolymerization rate is very high, there are not enough pushing barbed ends to generate a protrusive force (Figure S9). This means that increasing actin depolymerization can decrease the growth velocity (V_{mb} of the spine but not exert a contractile force. Therefore, when the net actin polymerization rate is reduced, as long as cofilin can generate barbed ends in the 'coherent' regime and myosin can generate contractile forces, then we can capture the observed dynamics. There are many factors that contribute to barbed end generation – polymerization, nucleation, and severing. If polymerization rate decreases, then the number of barbed ends with decrease, slowing down the velocity to zero and the spine volume will plateau out. But to shrink, an active inward pulling force is needed. We demonstrate that here with a simple system.

$$\frac{dR_{spine}}{dt} = V_{spine} - V_{\text{pulling by myosin}} \tag{S8}$$

Suppose that there is no pulling by myosin and the decrease in polymerization results in $V_{spine} = 0$. Then, we are left with $\frac{dR}{dt} = 0$ whose solution is a constant radius. Therefore, for the radius to shrink, an active pulling force is needed (Figure S10B).

Kinetic parameters

One of the challenges of developing models of signaling networks is choice of kinetic parameters. As the system of reactions gets more complex, it is harder to identify with certainty what a certain kinetic parameter value would be. One way to address this issue is to match the dynamics from simulations with experimental measurements of input-output relationships [21]. In this case, the data that is available is for the four key readouts in the spine and is available as percent change or normalized value. This makes it harder for us to identify kinetic parameters. We overcame this challenge by selecting kinetic parameters for the various reactions from the literature where possible and indicate it in the Tables. In some cases, the values of reaction rate constants were not available and these parameters were fit to match the experimental time course.

All chemical species, including actin had units of concentration in μM. The units of the kinetic parameters are as follows: all first order reaction rates and k_{cat}s have units of s^{-1}, second order reaction rates have units of $\mu M s^{-1}$, and K_m has units of μM. Barbed ends B and pushing barbed ends B_p have units of # and velocities V_0 and V_{mb} have units of $\mu m s^{-1}$. κ is the scale factor for converting concentrations to units of barbed ends and has units of $\#/\mu M$ [31]. Sensitivity analysis shows that the model is robust to changes in κ (Table S11).

Extracting experimental data from published work

The experimental data was extracted from Figure 1D of [19] using the digitize package in the software 'R' [24].

Model access in VCell

The simulations of the full network shown in Figure 2C were carried in the Virtual Cell program (http://www.nrcam.uchc.edu). The model is named 'Spine Model Final' and is available under the publicly shared models with the username 'prangamani'. Complete instructions on how access publicly shared models can be found at the Virtual Cell homepage. A teaching resource on how to develop models in Virtual Cell is given in [20].

Characteristics of the signaling cascade

In order to characterize the dynamics of the different protein activities and the volume change of the spine, we use the characteristics of the time-concentration or time-radius curve [9]. We use three measures of the curve to characterize the model output. (1) Time to peak signal – this is the time point at which maximum signal is achieved. (2) The area under the curve gives the total signal activated over the time of observation and for the i^{th} species is given by I_i in Eq. S9. (3) The signaling time is given by τ_i and gives the average duration of signal and is also defined in Eq. S9. These different values can be interpreted as the statistical measures of a time course in a signaling network (Table S9).

$$I_i = \int_0^\infty X_i(t)dt, \quad \text{and} \quad \tau_i = \frac{\int_0^\infty tX_i(t)dt}{I_i}. \tag{S9}$$

Tables

The references in these tables indicate either the source of the reaction and/or the source for the parameters. Often interaction parameters are given in terms of dissociation constants and these values were used to obtain the forward and backward rates for mass-action kinetics. In other cases, parameters were obtained from other models or assumed such that they would fit the experimental data.

Table S3: Reactions for the activation of CaMKII

Reaction	Reaction flux	Kinetic Parameters	Reference
$3Ca^{2+}$+ CaM → Ca·CaM	k_f[Ca^{2+}]^3[CaM]-k_r[Ca· CaM]	$k_f = 7.75$, $k_r = 1$	[23]
Ng + CaM → CaM·Ng	k_f[Ng][CaM]-k_r[Ca· CaM]	$k_f = 5$, $k_r = 1$	[36]
CaMKII + F-actin →CaMKII·F-actin	k_f[CaMKII][F-actin]-k_r[CaMKII]·[F-actin]	$k_f = 1$, $k_r = 4$	[29]
CaMKII + G-actin →CaMKII·G-actin	k_f[CaMKII][G-actin]-k_r[CaMKII]·[G-actin]	$k_f = 1$, $k_r = 4$	[29]
CaMKII → CaMKIIp	$\frac{k_{cat1}[\text{Ca·CaM}]^4[\text{CaMKII}]}{K_{m1}^4+[\text{Ca·CaM}]^4}$ + $\frac{k_{cat2}[\text{CaMKIIp}][\text{CaMKII}]}{K_{m2}+[\text{CaMKII}]}$	$k_{cat1} = 120$, K_{m1}=4, $k_{cat2} = 1$, $K_{m2} = 10$	[23]
CaMKIIp → CaMKII	$\frac{k_{cat}[\text{PP1*}][\text{CaMKIIp}]}{K_m+[\text{CaMKIIp}]}$	$k_{cat} = 15$, $K_m = 3$	[23]
CaN → CaN*	$\frac{k[\text{Ca·CaM}]^4[\text{CaN}]}{K_m^4+[\text{Ca·CaM}]^4}$	$k_{cat} = 127$, K_m=0.34	[36]
CaN* → CaN	$\frac{k_{cat}[\text{CaMKIIp}][\text{CaN}]}{K_m+[\text{CaN}]}$	$k_{cat} = 0.34$, $K_m = 127$	[36]
I1 → I1*	$\frac{k_{cat}[\text{CaN*}][\text{I1}]}{K_m+[\text{I1}]}$	$k_{cat} = 0.034$, K_m=4.97	[36]
I1* → I1	$\frac{k_{cat}[\text{CaMKIIp}][\text{I1*}]}{K_m+[\text{I1*}]}$	$k_{cat} = 0.0688$, $K_m = 127$	[36]
PP1 → PP1*	$\frac{k_{cat1}[\text{I1*}][\text{PP1}]}{K_{m1}+[\text{PP1}]}$ + $\frac{k_{cat2}[\text{PP1*}][\text{PP1}]}{K_{m2}+[\text{PP1}]}$	$k_{cat1} = 50$, K_{m1}=80, $k_{cat2} = 2$, $K_{m2} = 80$	[23]
PP1* → PP1	$\frac{k_{cat}[\text{CaMKIIp}][\text{PP1*}]}{K_m+[\text{PP1*}]}$	$k_{cat} = 0.07166$, $K_m = 4.97$	[36]

Table S4: Reactions for the activation of Cdc42 and Arp2/3

Reaction	Reaction flux	Kinetic Parameters	Reference
Cdc42-GEF → Cdc42-GEF*	$\frac{k_{cat}[\text{CaMKIIp}][\text{Cdc42-GEF}]}{K_m+[\text{Cdc42-GEF}]}$	$k_{cat} = 0.01$, $K_m = 1.0$	[37, 5], parameters estimated to match experimental time course
Cdc42-GEF* → Cdc42-GEF	$\frac{k_{cat}[\text{PP1*}][\text{Cdc42-GEF*}]}{K_m+[\text{Cdc42-GEF*}]}$	$k_{cat} = 0.01$, $K_m = 1.0$	[37, 5], parameters estimated to match experimental time course
Cdc42-GDP→ Cdc42-GTP	$\frac{k_{cat}[\text{Cdc42-GEF*}][\text{Cdc42-GDP}]}{K_m+[\text{Cdc42-GDP}]}$	$k_{cat} = 0.75$, $K_m = 1.0$	[37], parameters estimated to match experimental time course
Cdc42-GTP→ Cdc42-GDP	$\frac{k_{cat}[\text{GAP*}][\text{Cdc42-GTP}]}{K_m+[\text{Cdc42-GTP}]}$	$k_{cat} = 0.1$, $K_m = 1.0$	[37], parameters estimated to match experimental time course
GAP→ GAP*	$\frac{k_{cat}[\text{CaMKIIp}][\text{GAP}]}{K_m+[\text{GAP}]}$	$k_{cat} = 0.01$, $K_m = 1.0$	parameters estimated to match experimental time course
GAP*→ GAP	$\frac{k_{cat}[\text{PP1*}][\text{GAP*}]}{K_m+[\text{GAP*}]}$	$k_{cat} = 0.01$, $K_m = 1.0$	parameters estimated to match experimental time course
Cdc42-GTP + WASP → WASP*	$k_f[\text{Cdc42-GTP}][\text{WASP}]- k_r[\text{WASP*}]$	$k_f = 0.02$, $k_r = 0.001$	[15, 10, 26]
Arp2/3 + WASP* → Arp2/3*	$k_f[\text{Arp2/3}][\text{WASP*}] - k_r[\text{Arp2/3*}]$	$k_f = 0.1$, $k_r = 0.0$	[15, 10, 26]

Table S5: Reactions for the activation of Cofilin

Reaction	Reaction flux	Kinetic Parameters	Reference
SSH1 → SSH1*	$\frac{k_{cat}[\text{CaN*}][\text{SSH1}]}{K_m+[\text{SSH1}]}$	$k_{cat} = 0.34$, $K_m = 4.97$	[36]
SSH1* → SSH1	$\frac{k_{cat}[\text{CaMKII*}][\text{SSH1*}]}{K_m+[\text{SSH1*}]}$	$k_{cat} = 127$, $K_m = 0.34$	[23]
LIMK→ LIMK*	$\frac{k_{cat}[\text{ROCK*}][\text{LIMK}]}{K_m+[\text{LIMK}]}$	$k_{cat} = 0.9$, $K_m = 0.3$	[33]
LIMK*→ LIMK	$\frac{k_{cat}[\text{SSH1*}][\text{LIMK*}]}{K_m+[\text{LIMK*}]}$	$k_{cat} = 0.34$, $K_m = 4.0$	SSH1 was assumed to have similar kinetics as CaN; [36]
Cofilin→ Cofilin*	$\frac{k_{cat}[\text{SSH1*}][\text{Cofilin}]}{K_m+[\text{Cofilin}]}$	$k_{cat} = 0.34$, $K_m = 4.0$	SSH1 was assumed to have similar kinetics as CaN; [36]
Cofilin*→ Cofilin	$\frac{k_{cat}[\text{LIMK*}][\text{Cofilin*}]}{K_m+[\text{Cofilin*}]}$	$k_{cat} = 0.34$, $K_m = 4.0$	LIM Kinase was assumed to have similar parameters as CaMKII; [23]

Table S6: Reactions for the generation of actin barbed ends

Reaction	Reaction flux	Kinetic Parameters	Reference
F-new-actin → F-actin	$k_{age}[\text{F-new}]$	$k_{age} = 0.001$	[31]
F-actin → G-actin	$f_{sev} + k_{deg}[\text{F-actin}] + k_{depol}[\text{F-actin}]$	$k_{sev} = 0.0002$, $C_0 = 0.1$, $k_{depol} = 0.01$	[31]
	$f_{sev} = \frac{C_0 k_{sev}[\text{Cofilin*}]^4[\text{F-actin}]}{C_0^4}$	$k_{age} = 0.1$, $k_{deg} = 0.1$	
F-actin+G-actin+Arp23*→ F-actin	$f_{nuc} = \frac{k_{nuc}[\text{Arp23*}][\text{F-actin}][\text{G-actin}]}{K_m+[\text{Arp23*}]}$	$k_{nuc} = 15.3$, $K_m = 2$	[31]
→ B	$\kappa(f_{sev} + f_{nuc}) - k_{cap}B$	$k_{cap} = 0.04$, $\kappa = 106$	[31]
→ Bp	$(V_0 - V_{mb})B - k_{cap}Bp$	$V_0 = 0.1$, $k_{cap} = 0.04$	[31]

Table S7: Reactions for the activation of Rho and Myosin

Reaction	Reaction flux	Kinetic Parameters	Reference
Rho-GEF $\rightarrow$ Rho-GEF*	$\frac{k_{cat}[\text{CaMKIIp}][\text{Rho-GEF}]}{K_m+[\text{Rho-GEF}]}$	$k_{cat} = 0.01$, $K_m = 1.0$	Est.
Rho-GEF* $\rightarrow$ Rho-GEF	$\frac{k_{cat}[\text{PP1*}][\text{Rho-GEF*}]}{K_m+[\text{Rho-GEF*}]}$	$k_{cat} = 0.1$, $K_m = 1.0$	Est.
Rho-GDP$\rightarrow$ Rho-GTP	$\frac{k_{cat}[\text{Rho-GEF*}][\text{Rho-GDP}]}{K_m+[\text{Rho-GDP}]}$	$k_{cat} = 0.75$, $K_m = 1.0$	Est.
Rho-GTP$\rightarrow$ Rho-GDP	$\frac{k_{cat}[\text{GAP*}][\text{Rho-GTP}]}{K_m+[\text{Rho-GTP}]}$	$k_{cat} = 0.1$, $K_m = 1.0$	Est.
Rho-GTP + ROCK $\rightarrow$ ROCK*	$k_f[Rho-GTP][ROCK] - k_r[ROCK*]$	$k_f = 0.02$, $k_r = 0.001$	[26]
MyoPpase$\rightarrow$ MyoPpase*	$k_f[MyoPpase] + \frac{k_{cat}[\text{MyoPpase*}][\text{MyoPpase}]}{K_m+[\text{MyoPpase}]}$	$k_f = 0.01$, $k_{cat} = 3$, $K_m = 16$	[12]
MyoPpase* $\rightarrow$ MyoPpase	$\frac{k_{cat}[\text{ROCK*}][\text{MyoPpase*}]}{K_m+\text{MyoPpase*}]}$	$k_{cat} = 2.357$, $K_m = 0.1$	[12]
MLC$\rightarrow$ MLC*	$k_f[MLC] + \frac{k_{cat}[\text{ROCK*}][\text{MLC}]}{K_m+[\text{MLC}]}$	$k_f = 0.01$, $k_{cat} = 1.8$, $K_m = 2.47$	[12]
MLC* $\rightarrow$ MLC	$\frac{k_{cat}[\text{MyoPPase*}][\text{MLC*}]}{K_m+\text{MLC*}]}$	$k_{cat} = 1$, $K_m = 16$	[12]

Table S8: Initial conditions (only the species with non-zero initial conditions are shown)

Species	Initial concentration (μM)	Notes and References
CaMKII-F-actin	10	Assumed based on [22]; varied in our simulations (Figure S4)
CaMKII-G-actin	10	Assumed based on [22]; varied in our simulations (Figure S4)
Calcineurin	1	[36]; varied in our simulations (Figure S4)
Calmodulin	10	[36]; varied in our simulations (Figure S4)
Neurogranin	20	[36]
I1	1.8	[36]; varied in our simulations (Figure S3)
LIM kinase	2	Assumed
Myoppase*	0.1	[12]
RhoGEF	0.1	Assumed
RhoGAP	0.1	Assumed
Cdc42GEF	0.1	Assumed
PP1	0.27	Estimated by parameter variation (Figure S3)
ROCK	1.0	Assumed; varied in our simulations (Figure S6)
RhoGDP	1.0	Assumed; varied in our simulations (Figure S6)
WASP	1.0	Assumed
Arp2/3	1.0	Assumed; varied in our simulations (Figure S5)
Cdc42GDP	1.0	Assumed; varied in our simulations (Figure S5)
Bp	1.0	Set to a small non-zero value to initiate simulations
Myoppase	1.1	[12]
SSH1	2.0	Assumed
Cofilin	2.0	Assumed; varied in our simulations (Figure S5)
MLC	5.0	[12]; varied in our simulations (Figure S6)
B	30.0	[31]; set to a small resting value to indicate that most of the actin is bundled to CaMKII

Table S9: Characteristics of different species in the signaling cascade

Species	Signal exposure I	Signal Duration τ(s)	Time to peak(s)	RMSE for model-experiment comparison
CaMKII	66.67	44.1	13	0.11
Rho	159.48	117.2	48	0.04
Cdc42	167	130.31	51	0.25
Spine volume	184	150.62	102	0.04

Table S10: Sensitivity to initial conditions

Index	Component	CaMKII	Cdc42	Rho	Radius
1	Cofilin	✓	X	X	X
2	Arp23	✓	X	X	X
3	CaN	✓	X	X	X
4	CaMKII-Factin	✓	X	✓	X
5	CaMKII-Gactin	✓	X	✓	X
6	Cdc42GTP	✓	✓	X	X
7	Cdc42 GEF	X	X	X	X
8	I1	X	X	✓	✓
9	LIMK	✓	X	X	X
10	MLC	X	X	X	X
11	Myoppase active	X	X	X	X
12	Myoppase	✓	X	X	X
13	Ng	✓	X	X	X
14	PP1	✓	X	✓	X
15	RhoGAP	X	X	X	X
16	RhoGEF	X	X	X	X
17	RhoGDP	X	X	X	X
18	ROCK	X	X	✓	✓
19	SSh1	✓	X	X	✓
20	WASP	✓	✓	X	X

Table S11: Sensitivity to kinetic parameters

Index	Name	CaMKII	Cdc42	Rho	Radius	Index	Name	CaMKII	Cdc42	Rho	Radius
1	k_{age}	X	X	X	X	41	k_f ROCK inactivation	X	X	X	X
2	V_0	X	X	X	✓	42	K_m for CaMKII activation	X	X	X	X
3	ω	X	X	X	X	43	K_{m1} for CaMKII autoactivation	X	X	X	X
4	k_{cap}	X	X	X	✓	44	K_{m1} for PP1 activation by I1	X	X	X	X
5	k_{deg}	X	X	X	X	45	K_{m2} for PP1 autoactivation	X	X	X	X
6	k_{nuc}	X	X	X	X	46	K_m for CaN activation by CaM	X	X	X	X
7	k_{sev}	X	X	X	X	47	K_m for CaN inactivation	X	X	X	X
8	k_{shrink}	X	X	X	X	48	K_m for CaMKII inactivation by CaM	X	X	X	X
9	κ	X	X	X	X	49	K_m for CaMKII inactivation	✓	X	✓	X
10	k_f for Arp2/3 inactivation	X	X	X	X	50	K_m Cdc42 activation	X	X	X	X
11	k for CaN activation by CaM	X	X	X	X	51	K_m Cdc42GEFactivation	X	X	X	X
12	k_{cat} for PP1 activation by I1	X	X	X	X	52	K_m Cdc42GEF inactivation	✓	X	X	X
13	k_{cat} for PP1 autodephosphorylation	X	X	X	X	53	K_m for Cdc42 hydrolysis	X	X	X	X
14	k_{cat} for CaMKII activation by CaM	X	X	X	X	54	K_m cofilin activation SSH1	X	X	X	X
15	k_{cat} CaMKII autophoshorylation	✓	X	X	X	55	K_m I1 activation by CaN	X	X	X	X
16	k_{cat} CaMKII inactivation by PP1	✓	X	✓	X	56	K_m I1 inactivation	X	X	X	X
17	k_{cat} Cdc42 activation by GEF	X	X	X	X	57	K_m LIMK activation by ROCK	X	X	X	X
18	k_{cat} Cdc42GEF activation by CaMKII	X	X	X	X	58	k_m LIMK inactivation by SSH1	X	X	X	X
19	k_{cat} Cdc42GEF inactivation by PP1	X	X	X	X	59	K_m MLC dephosphorylation	X	X	X	X
20	k_{cat} Cdc42 hydrolysis	X	X	X	X	60	K_m Myoppase activation	X	X	X	X
21	k_{cat} Cofilin activation by SSH1	X	X	X	X	61	K_m Myoppase inactivation	X	X	X	X
22	k_{cat} Cofilin inactivation by LIMK	X	X	X	X	62	K_m PP1 inactivation by CaMKII	X	X	X	X
23	k_{cat} I1 inactivation by CaMKII	X	X	X	X	63	K_m RhoGEF inactivation	X	X	X	X
24	k_{cat} LIMK activation by ROCK	X	X	X	X	64	K_m RhoGAP activation by CaMKII	X	X	X	X
25	k_{cat} MLC phosphorylation by ROCK	X	X	X	X	65	K_m RhoGAP inactivation by PP1	X	X	X	X
26	k_{cat} Myoppase dephosphorylation	X	X	X	X	66	K_m RhoGEF activation by CaMKII	X	X	X	X
27	k_{cat} Myoppase inactivation by ROCK	X	X	X	X	67	K_m RhoGTP by RhoGEF	X	X	X	X
28	k_{cat} PP1 inactivation by CaMKII	X	X	X	X	68	K_m RhoGTP hydrolysis	X	X	X	X
29	k_{cat} RhoGAP activation by CaMKII	X	X	X	X	69	K_m SSH1 dephosphorylation	X	X	X	X
30	k_{cat} RhoGEF activation by CaMKII	X	X	X	X	70	K_m SSH1 phosphorylation by CaMKII	X	X	X	X
31	k_{cat} RhoGEF activity	X	X	X	X	71	k_r for Ca^{2+}CaM binding	X	X	X	X
32	k_f Ca^{2+}CaM binding	✓	X	X	X	72	k_r Arp2/3 activation	X	X	X	X
33	k_f Arp2/3 activation	X	X	X	X	73	k_r CaM binding Ng	X	X	X	X
34	k_f CaM Ng binding	X	X	X	X	74	k_r CaMKII binding F-actin	X	X	X	X
35	k_f CaMKII-F-actin binding	X	X	X	X	75	k_r CaMKII G-actin	X	X	X	X
36	k_f CaMKII-G-actin binding	X	X	X	X	76	k_r Cdc42 WASP bidning	X	X	X	X
37	k_f WASP activation by Cdc42	X	X	X	X	77	k_r MLCp basal activity	X	X	X	X
38	k_f MLC phosphorylation	X	X	X	X	78	k_r Myoppase basal activity	X	X	X	X
39	k_f Myoppase basal activity	X	X	X	X	79	k_r ROCK activation by Rho	X	X	X	X
40	k_f ROCK activation by Rho	X	X	X	X	80	k_r ROCK inactivation	X	X	X	X

Figures

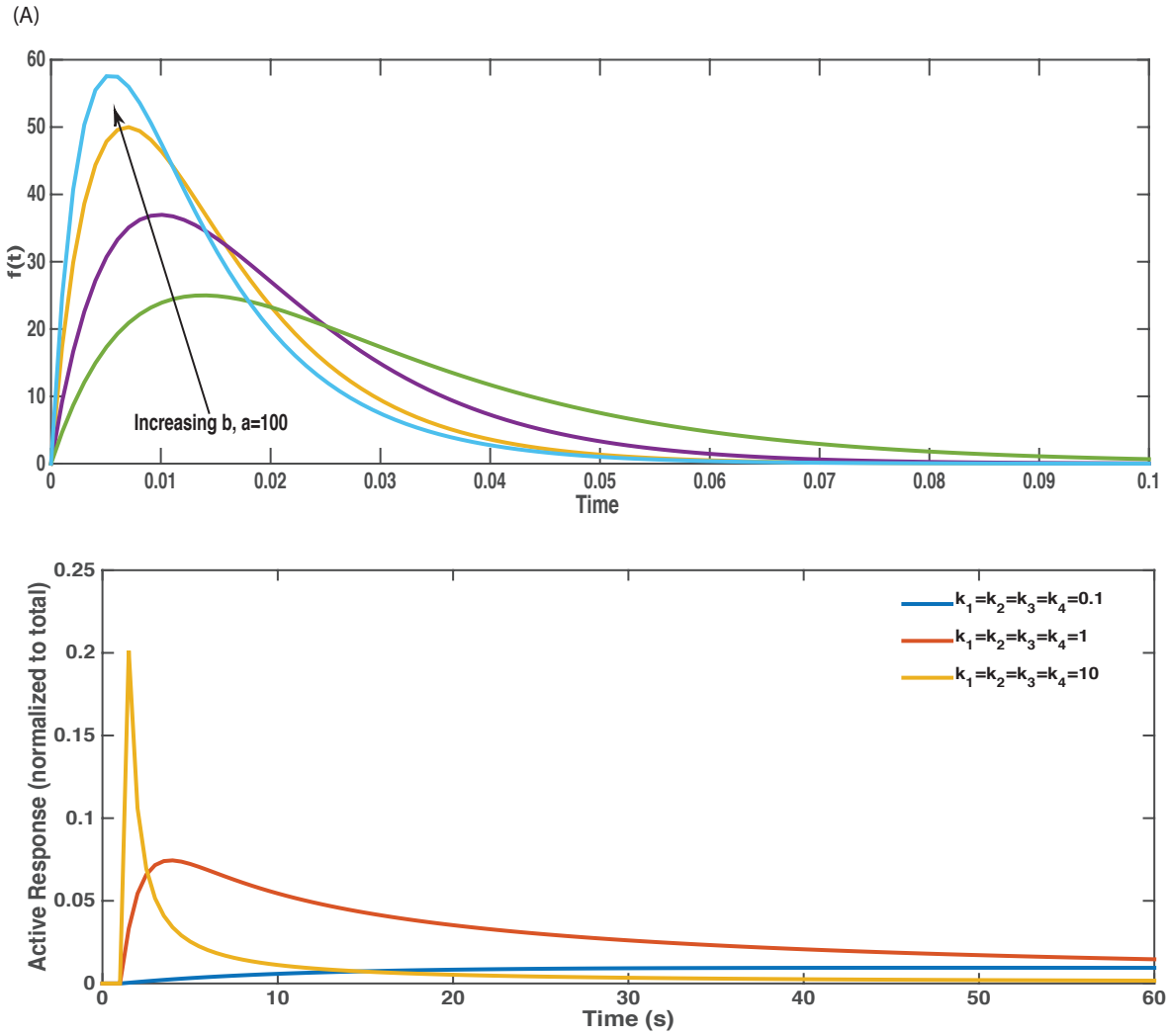

Figure S1: (A) The parameters of a biexponential function $f(t)$ can be tuned to change the dynamics of the function. This simple model shows how dynamics of the response function can be controlled by simple parameters. By tuning the parameters, a and b, of the function, we can capture the fast response that is like that of CaMKII and a slow-response that is like the spine volume. (B) The role of parameters in governing the dynamics of the simple paradoxical signaling module is shown. Changing the parameters captures the full range of behavior.

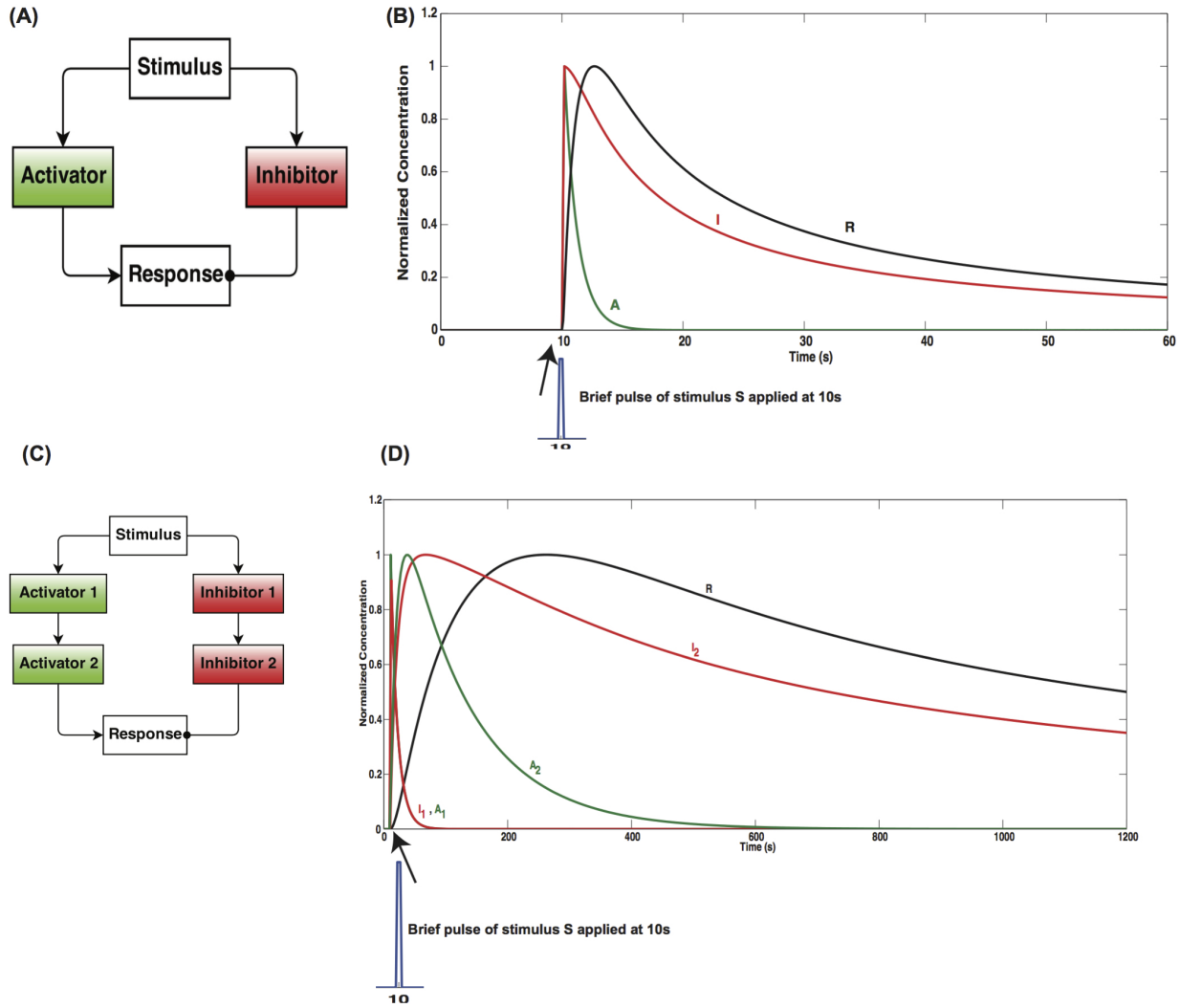

Figure S2: (A) An activation inhibition loop governed by the same stimulus S leads to the dynamics of the response R as shown in (B). This is an example of paradoxical signaling. In this network structure, the temporal dynamics of the response R can be regulated by a biexponential function (Figure S1) in the supplemental material, where the exponential associated with the increase of R is controlled by the activator and the exponential associated with the decay of R is controlled by the inhibitor. Tuning the effect of the exponentials is enough to move the peak of the response curve (see supplemental material for a detailed discussion). The multi-level activation inhibition loop in Figure 2B can be represented by a toy model as shown in (C). The time course of the response R is dependent on the number of upstream tiers, essentially resulting in biexponential functions of exponentials. The first level of activator and inhibitor show an early response, the second activator and inhibitor show an intermediate time course and the response R shows a delay compared to the stimulus presented at 10 s. This indicates that multi-tiered activation-inhibition networks of paradoxical signaling are sufficient to control the temporal evolution of the response.

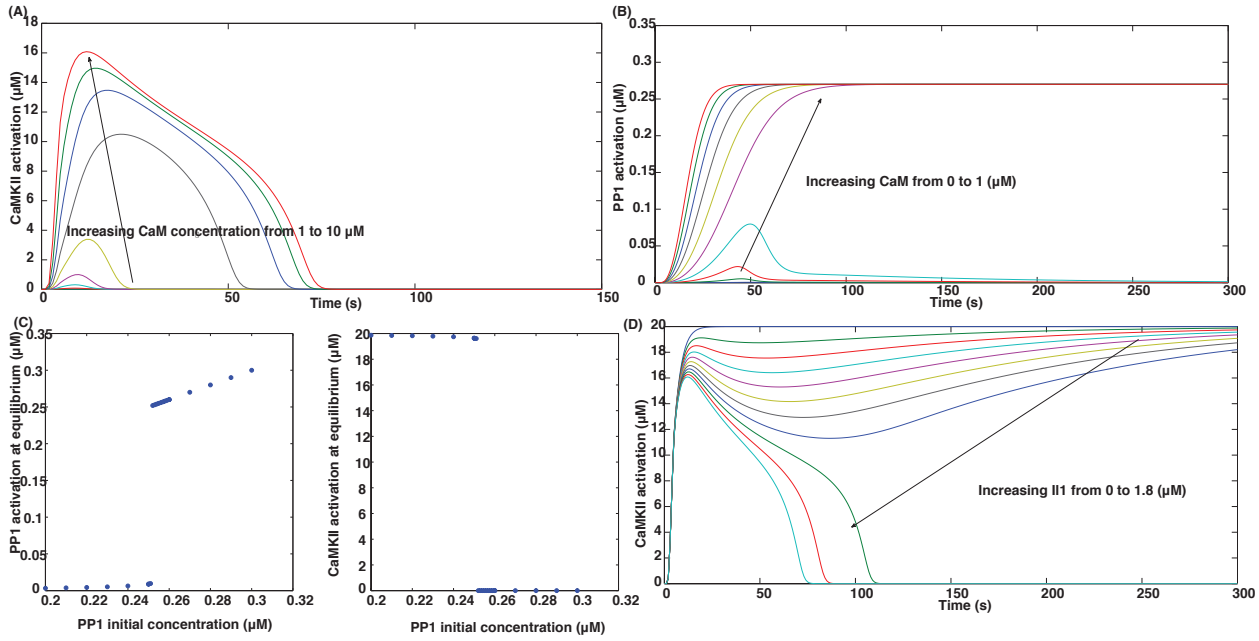

Figure S3: (A) CaMKII dynamics depends on the amount of CaM. If the concentration of CaM is low, not enough CaMKII is activation through phosphorylation. (B) PP1 dynamics is also affected by CaM. For very low amounts of CaM, PP1 activation is not enough to dephosphorylate CaMKII and it results in sustained CaMKII activation. (C) Ultrasensitivity of PP1 and CaMKII activation on PP1 initial concentration. The series of phosphatases (CaN, I1, and CaMKII) coupled with autophosphorylation of CaMKII, and autodephosphorylation of PP1 gives rise to ultrasensitive responses. (D) Increasing I1 concentration also affects CaMKII activation – low concentration of I1 results in sustained activation of CaMKII and high concentration of I1 results in transient activation of CaMKII.

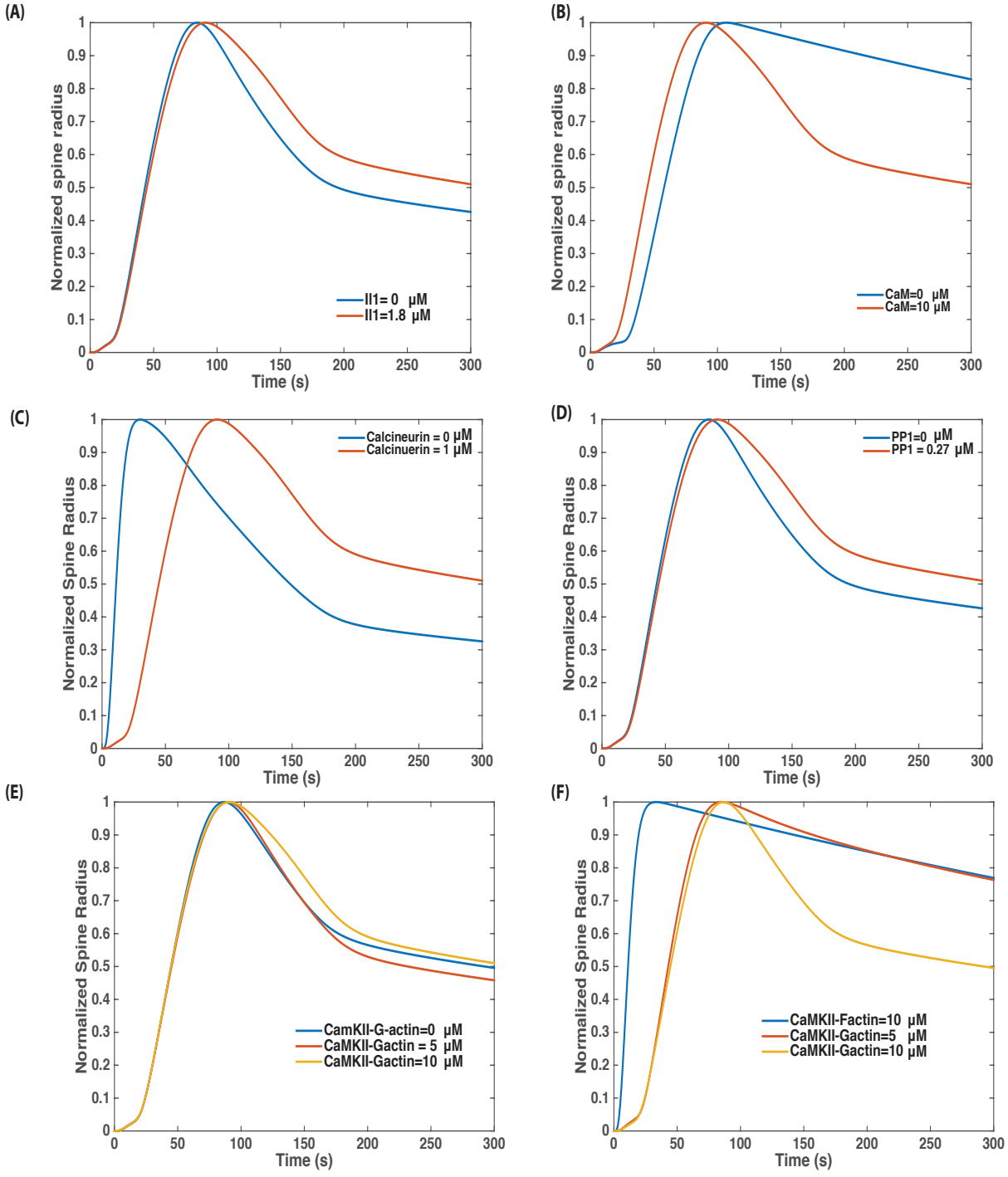

Figure S4: Effect of the components of the CaMKII module on spine radius change. Note that the normalized spine radius is shown and does not reflect the absolute change in the radius of the spine. Effect of I1 concentration (A) , PP1 (D) , and CaMKII-G-actin (E) on spine radius is small. As we explain in later sections, the dynamics downstream of these components is governed by the generation of actin barbed ends and the effect of these components is mitigated by other interactions in the network. On the other hand CaM (B), CaN (C), and CaMKII-F-actin (F) concentrations have significant impact on spine radius change.

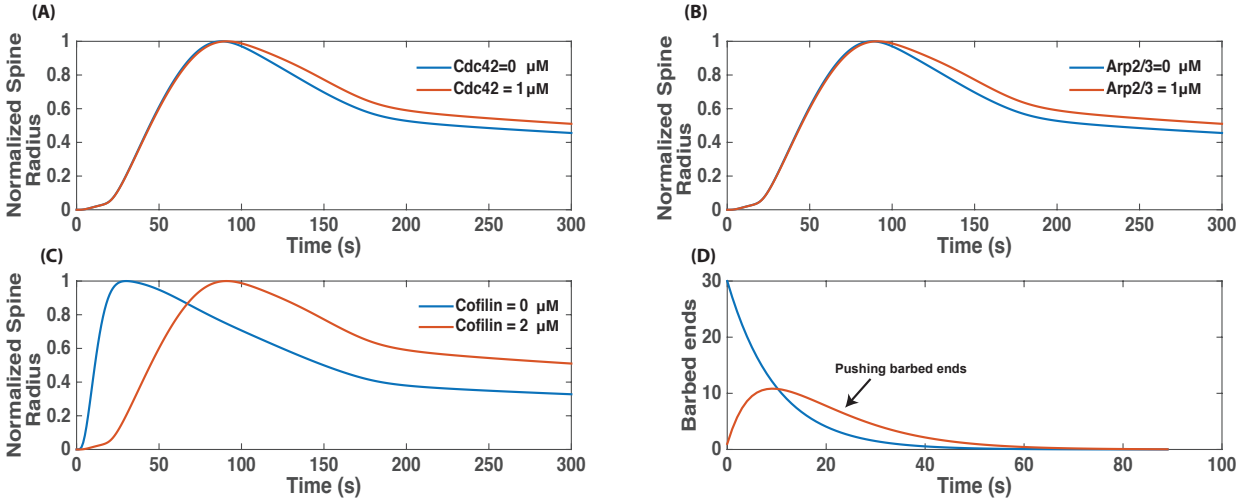

Figure S5: Effect of Cdc42 and related components on spine volume change. (A) From first observations, it seems that Cdc42 alone does not have a significant effect on the spine volume change. (B) Similarly, Arp2/3 alone does not have a strong effect on spine volume change. (C) However, cofilin has a significant effect on spine volume dynamics. This is a case where the model indicates that the complex interactions of the actin network are important for governing the dynamics of the dendritic spine. (D) When both cofilin and Arp2/3 are removed, the number of barbed ends and pushing barbed ends falls to zero very rapidly since all barbed ends get capped.

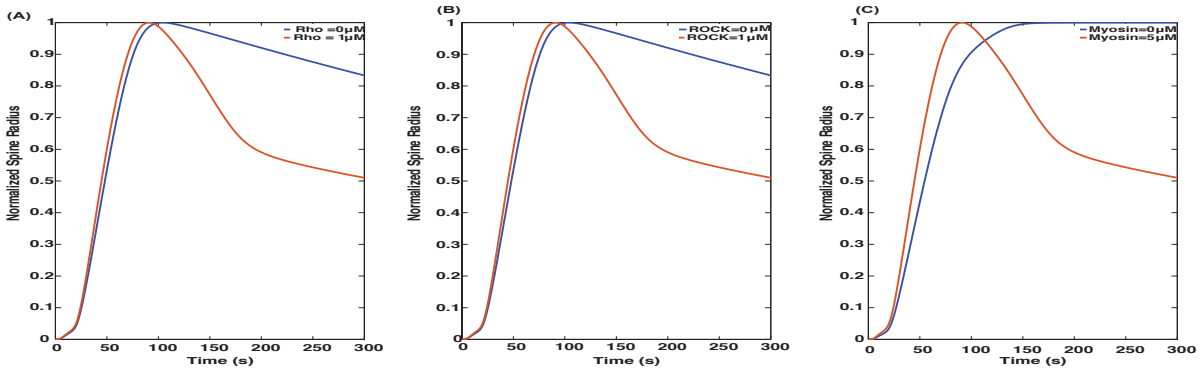

Figure S6: Effect of Rho and related components on spine volume change. (A) Rho is required for maintaining the dynamics of spine volume decrease; note that there is no effect on the increase in spine volume. (B) Rho-kinase is also important for maintaining the dynamics of spine volume decrease. (C) Myosin is the key component for governing the decrease in spine volume. Absence of myosin results in a sustained increase in spine volume.

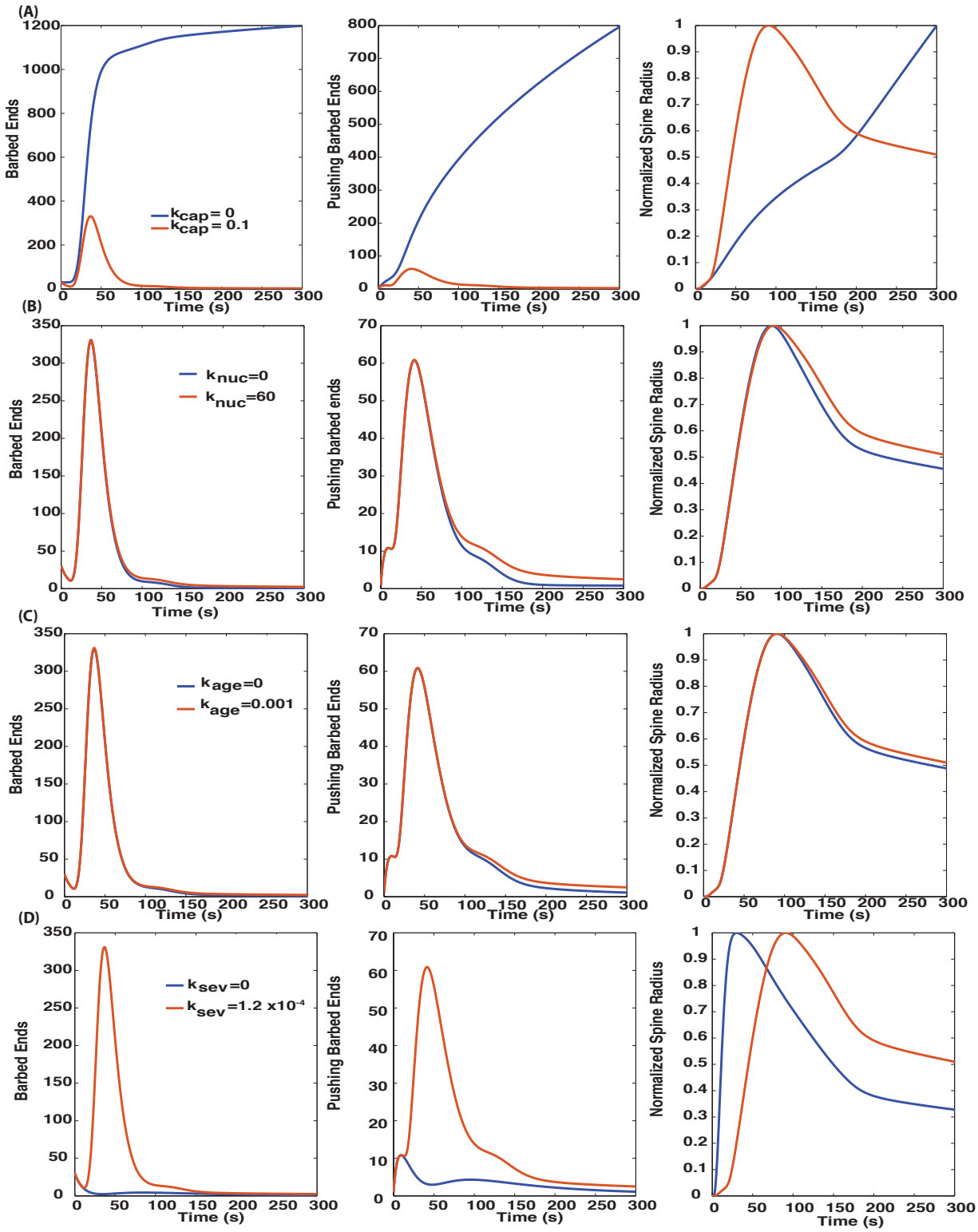

Figure S7: Effect of actin remodeling. (A) Capping rate is an important aspect of controlling spine dynamics. Setting k_{cap} to zero results in a large increase in barbed ends, pushing barbed ends, and spine radius. (B) Filament nucleation rate k_{nuc} and (C) filament aging k_{age} do not have a significant impact on barbed ends, pushing barbed ends, and spine radius. (D) Filament severing rate k_{sev} plays an important role in governing barbed end and spine dynamics. These predictions can be tested using pharmacological treatments in the laboratory.

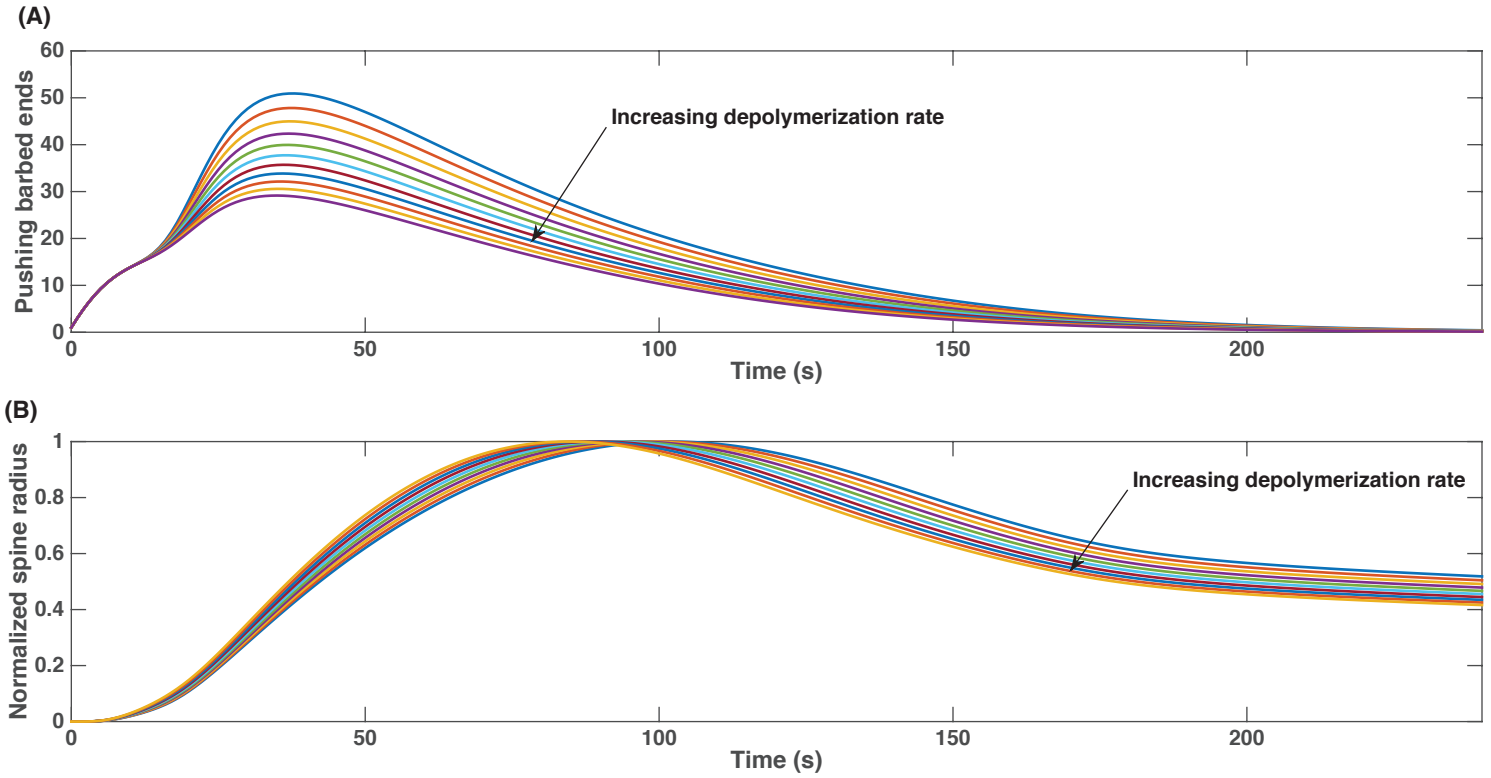

Figure S8: Role of actin depolymerization. We tested the effect of increasing depolymerization rate on pushing barbed end generation and spine radius change. (A) Increase the depolymerization rate from 0 to 0.1 s^{-1} reduced the number of pushing barbed ends. (B) For the same values of the depolymerization rate, the spine radius did not change very much because the system was in the 'coherent' regime.

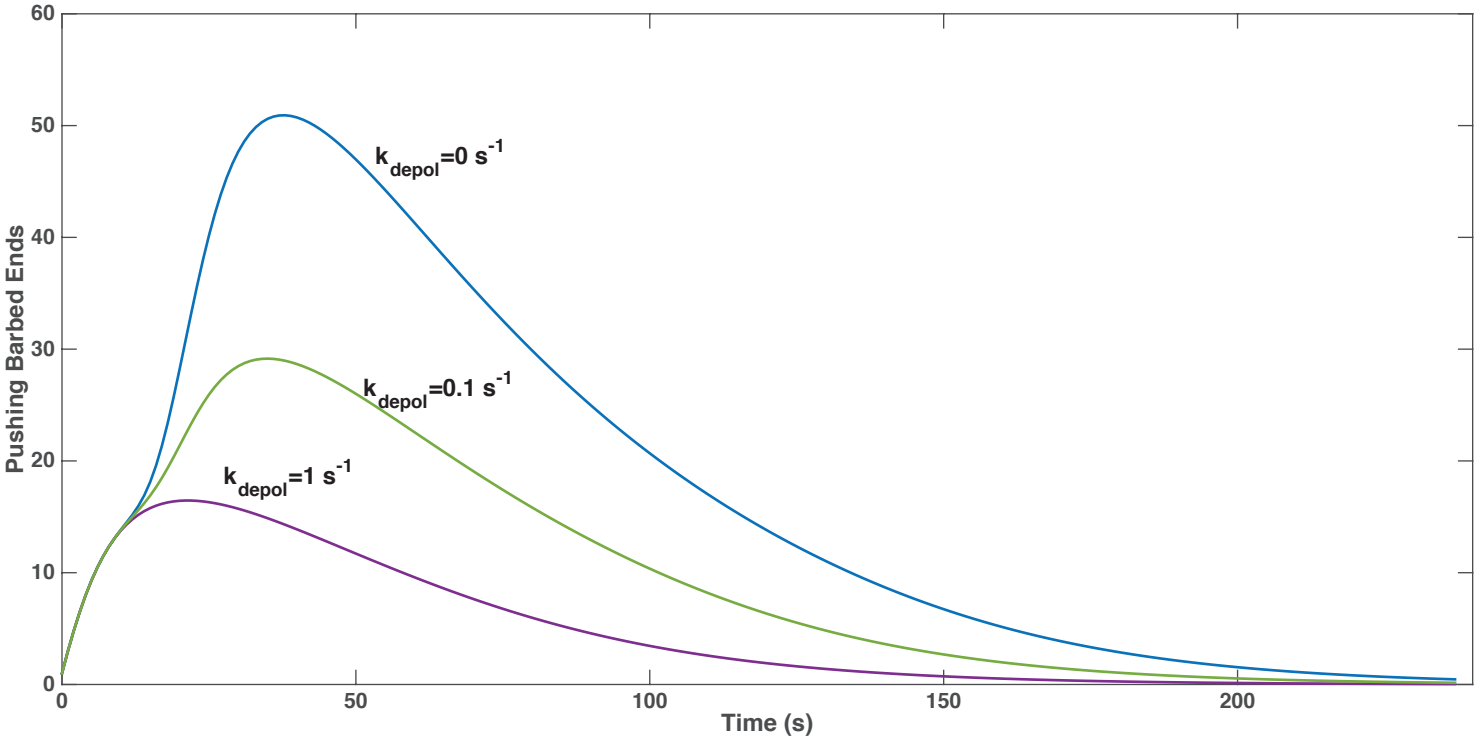

Figure S9: Effect of depolymerization rate on pushing barbed ends. Increasing the depolymerization rate decreases the number of pushing barbed ends. When the depolymerization rate is very high, there are very few pushing barbed ends available to generate a protrusive velocity.

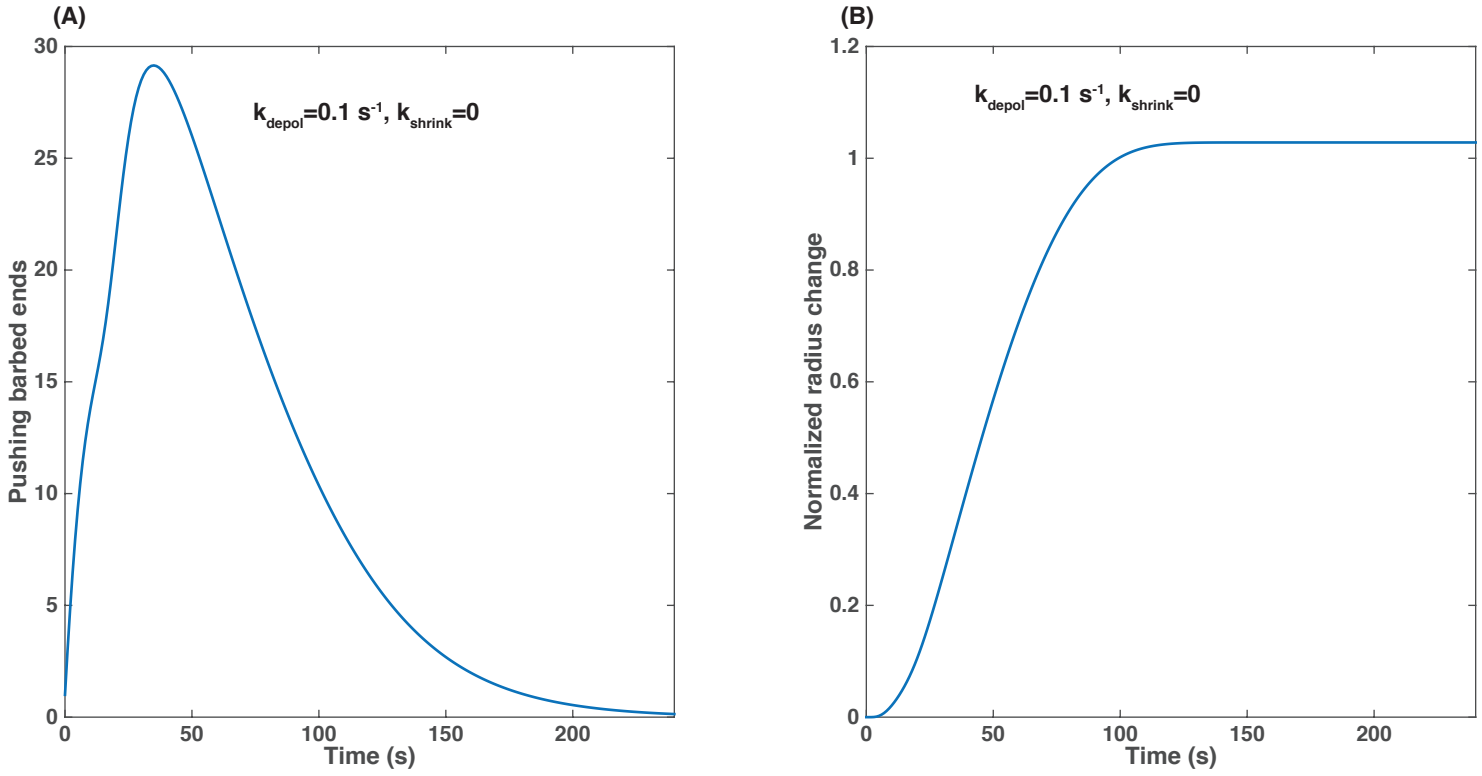

Figure S10: Actin depolymerization or myosin-contraction? If only actin depolymerization is included in the model with no myosin-mediated contraction, then (A) the pushing barbed ends are still generated and (B) increase the spine radius, but the spine radius does not decrease.

References

[1] Uri Alon. Network motifs: theory and experimental approaches. *Nature Reviews Genetics*, 8(6):450–461, 2007.

[2] Mutsuki Amano, Masanori Nakayama, and Kozo Kaibuchi. Rho-kinase/rock: a key regulator of the cytoskeleton and cell polarity. *Cytoskeleton*, 67(9):545–554, 2010.

[3] Erin Barnhart, Kun-Chun Lee, Greg Allen, Julie Theriot, and Alex Mogilner. Balance between cell-substrate adhesion and myosin contraction determines the frequency of motility initiation in fish keratocytes. *Proceedings of the National Academy of Sciences*, 112(18):5045, 2015.

[4] Mitsuharu Endo, Kazumasa Ohashi, Yukio Sasaki, Yoshio Goshima, Ryusuke Niwa, Tadashi Uemura, and Kensaku Mizuno. Control of growth cone motility and morphology by lim kinase and slingshot via phosphorylation and dephosphorylation of cofilin. *The Journal of neuroscience*, 23(7):2527–2537, 2003.

[5] Ian N Fleming, Cassondra M Elliott, F Gregory Buchanan, C Peter Downes, and John H Exton. Ca2+/calmodulin-dependent protein kinase ii regulates tiam1 by reversible protein phosphorylation. *Journal of Biological Chemistry*, 274(18):12753–12758, 1999.

[6] Jonathan Goldberg, Angus C Nairn, and John Kuriyan. Structural basis for the autoinhibition of calcium/calmodulin-dependent protein kinase i. *Cell*, 84(6):875–887, 1996.

[7] Yuval Hart and Uri Alon. The utility of paradoxical components in biological circuits. *Molecular cell*, 49(2):213–221, 2013.

[8] Yuval Hart, Yaron E Antebi, Avraham E Mayo, Nir Friedman, and Uri Alon. Design principles of cell circuits with paradoxical components. *Proceedings of the National Academy of Sciences*, 109(21):8346–8351, 2012.

[9] Reinhart Heinrich, Benjamin G Neel, and Tom A Rapoport. Mathematical models of protein kinase signal transduction. *Molecular cell*, 9(5):957–970, 2002.

[10] Henry N Higgs and Thomas D Pollard. Activation by cdc42 and pip2 of wiskott-aldrich syndrome protein (wasp) stimulates actin nucleation by arp2/3 complex. *The Journal of cell biology*, 150(6):1311–1320, 2000.

[11] Naoki Honkura, Masanori Matsuzaki, Jun Noguchi, Graham CR Ellis-Davies, and Haruo Kasai. The subspine organization of actin fibers regulates the structure and plasticity of dendritic spines. *Neuron*, 57(5):719–729, 2008.

[12] Takako Kaneko-Kawano, Fugo Takasu, Honda Naoki, Yuichi Sakumura, Shin Ishii, Takahiro Ueba, Akinori Eiyama, Aiko Okada, Yoji Kawano, and Kenji Suzuki. Dynamic regulation of myosin light chain phosphorylation by rho-kinase. *PloS one*, 7(6):e39269–e39269, 2012.

[13] Farida Korobova and Tatyana Svitkina. Molecular architecture of synaptic actin cytoskeleton in hippocampal neurons reveals a mechanism of dendritic spine morphogenesis. *Molecular biology of the cell*, 21(1):165–176, 2010.

[14] Catherine I Lacayo, Zachary Pincus, Martijn M VanDuijn, Cyrus A Wilson, Daniel A Fletcher, Frank B Gertler, Alex Mogilner, and Julie A Theriot. Emergence of large-scale cell morphology and movement from local actin filament growth dynamics. *PLoS Biol*, 5(9):e233, 2007.

[15] Jean-Baptiste Marchand, Donald A Kaiser, Thomas D Pollard, and Henry N Higgs. Interaction of wasp/scar proteins with actin and vertebrate arp2/3 complex. *Nature cell biology*, 3(1):76–82, 2001.

[16] Alex Mogilner and George Oster. Force generation by actin polymerization ii: the elastic ratchet and tethered filaments. *Biophysical journal*, 84(3):1591–1605, 2003.

[17] Alexander Mogilner and George Oster. Cell motility driven by actin polymerization. *Biophysical journal*, 71(6):3030, 1996.

[18] Rosel M Mulkey, Shogo Endo, Shirish Shenolikar, and Robert C Malenka. Involvement of a calcineurin/inhibitor-1 phosphatase cascade in hippocampal long-term depression. *Nature*, 369(6480):486–488, 1994.

[19] Hideji Murakoshi and Ryohei Yasuda. Postsynaptic signaling during plasticity of dendritic spines. *Trends in neurosciences*, 35(2):135–143, 2012.

[20] Susana R Neves. Developing models in virtual cell. *Science signaling*, 4(192):tr12, 2011.

[21] Susana R Neves. Obtaining and estimating kinetic parameters from the literature. *Science signaling*, 4(191):tr8, 2011.

[22] Kenichi Okamoto, Miquel Bosch, and Yasunori Hayashi. The roles of camkii and f-actin in the structural plasticity of dendritic spines: a potential molecular identity of a synaptic tag? *Physiology*, 24(6):357–366, 2009.

[23] Hyun Jae Pi and John E Lisman. Coupled phosphatase and kinase switches produce the tristability required for long-term potentiation and long-term depression. *The Journal of Neuroscience*, 28(49):13132–13138, 2008.

[24] Timothée Poisot. The digitize package: extracting numerical data from scatterplots. *The R Journal*, 3(1):25–26, 2011.

[25] Thomas D Pollard. Rate constants for the reactions of atp-and adp-actin with the ends of actin filaments. *The Journal of cell biology*, 103(6):2747–2754, 1986.

[26] Padmini Rangamani, Marc-Antoine Fardin, Yuguang Xiong, Azi Lipshtat, Olivier Rossier, Michael P Sheetz, and Ravi Iyengar. Signaling network triggers and membrane physical properties control the actin cytoskeleton-driven isotropic phase of cell spreading. *Biophysical journal*, 100(4):845–857, 2011.

[27] Rajat Rohatgi, Le Ma, Hiroaki Miki, Marco Lopez, Tomas Kirchhausen, Tadaomi Takenawa, and Marc W Kirschner. The interaction between n-wasp and the arp2/3 complex links cdc42-dependent signals to actin assembly. *Cell*, 97(2):221–231, 1999.

[28] Oren S Rosenberg, Sebastian Deindl, Rou-Jia Sung, Angus C Nairn, and John Kuriyan. Structure of the autoinhibited kinase domain of camkii and saxs analysis of the holoenzyme. *Cell*, 123(5):849–860, 2005.

[29] Hugo Sanabria, Matthew T Swulius, Steven J Kolodziej, Jun Liu, and M Neal Waxham. βcamkii regulates actin assembly and structure. *Journal of Biological Chemistry*, 284(15):9770–9780, 2009.

[30] Patrick D Sarmiere and James R Bamburg. Regulation of the neuronal actin cytoskeleton by adf/cofilin. *Journal of neurobiology*, 58(1):103–117, 2004.

[31] Nessy Tania, John Condeelis, and Leah Edelstein-Keshet. Modeling the synergy of cofilin and arp2/3 in lamellipodial protrusive activity. *Biophysical journal*, 105(9):1946–1955, 2013.

[32] Vedakumar Tatavarty, Eun-Ji Kim, Vladimir Rodionov, and Ji Yu. Investigating sub-spine actin dynamics in rat hippocampal neurons with super-resolution optical imaging. *PloS one*, 4(11):e7724, 2009.

[33] John W Trauger, Fen-Fen Lin, Mary S Turner, Jeffrey Stephens, and Philip V LoGrasso. Kinetic mechanism for human rho-kinase ii (rock-ii). *Biochemistry*, 41(28):8948–8953, 2002.

[34] David M Virshup and Shirish Shenolikar. From promiscuity to precision: protein phosphatases get a makeover. *Molecular cell*, 33(5):537–545, 2009.

[35] Yan Wang, Futoshi Shibasaki, and Kensaku Mizuno. Calcium signal-induced cofilin dephosphorylation is mediated by slingshot via calcineurin. *Journal of Biological Chemistry*, 280(13):12683–12689, 2005.

[36] Anatol M Zhabotinsky, R Nicholas Camp, Irving R Epstein, and John E Lisman. Role of the neurogranin concentrated in spines in the induction of long-term potentiation. *The Journal of neuroscience*, 26(28):7337–7347, 2006.

[37] Baolin Zhang, Zhi-Xin Wang, and Yi Zheng. Characterization of the interactions between the small gtpase cdc42 and its gtpase-activating proteins and putative effectors comparison of kinetic properties of cdc42 binding to the cdc42-interactive domains. *Journal of Biological Chemistry*, 272(35):21999–22007, 1997.